Energy loss of H^+ fragments arising from dissociation of fast H_2^+ ions under glancing-angle incidence on a SnTe(001) surface

Y. Susuki
Department of Physics, Osaka Kyoiku University, Kashiwara, Osaka 582, Japan
(Received 10 March 1997)

Energy losses of H^+ fragments repelled parallel and antiparallel to the beam direction at dissociation are measured for a glancing-angle incidence of 0.15–0.6-MeV/amu H_2^+ ions on a clean (001) surface of SnTe. The sum of the energy losses of the specularly reflected fragments is larger than twice that of protons of the same velocity reflected from the surface. For the interpretation of the vicinage effect on the stopping power of the surface, the energy losses of the pairs of fragments resulting from the dissociation of H_2^+ are calculated at the glancing-angle scattering. The contribution of single-electron excitation to the energy loss of the pair is calculated with the harmonic-oscillator model [J. Basbas and R. H. Ritchie, Phys. Rev. A **25**, 1943 (1982)] and that of collective excitation by the superposition of surface wakes of two protons. A dependence of the vicinage effect on the distance from the surface is found from the calculated stopping powers, where the pronounced effect becomes weak as the distance decreases. The calculated energy losses of the reflected pairs of protons agree fairly with those measured. The agreement of the calculated energy losses with those measured supports the calculated dependence of the vicinage effects. [S1050-2947(97)07810-4]

PACS number(s): 79.20.Rf, 34.50.Gb, 34.70.+e, 34.80.Gs

I. INTRODUCTION

The investigation of dissociation of energetic molecular ions incident on a solid is of considerable importance in a number of applications, e.g., cluster fusion and cluster ion deposition. When a MeV or sub-MeV H_2^+ molecular ion impinges on a foil, a binding electron of the H_2^+ is stripped off rapidly by a collision with the target atom and the remaining two protons dissociate via a mutual Coulomb force in the solid. This is referred to as ''Coulomb explosion.'' The laboratory system velocities of fragments shift from the velocity of incidence due to the Coulomb explosion. Since the velocity shift is a function of the angle between the molecular axis and the incident beam direction, the H^+ fragments arising from the breakup of randomly oriented H_2^+ ions form a ring pattern in a joint distribution of energy and angle [1–3].

The energies of the two fragments arising from the breakup of a MeV H_2^+ ion in a foil, whose molecular axis tilts by an angle Θ with respect to the beam direction, are given by

$$E_L = \tfrac{1}{2} M_p V^2 + M_p V v_c \cos\Theta - \Delta E_L ,$$
$$E_T = \tfrac{1}{2} M_p V^2 - M_p V v_c \cos\Theta - \Delta E_T , \tag{1}$$

where E_L and E_T are the energies of the leading and trailing fragments, respectively, M_p is the proton mass, V is the projectile velocity, v_c is the asymptotic center-of-mass (c.m.) system velocity of the fragment acquired by the Coulomb explosion, and $\Delta E_M = \Delta E_L + \Delta E_T$ is the energy loss of the pair of fragments. For MeV H_2^+ projectiles, V is more than 100 times larger than v_c.

Since the work by Brandt, Ratkowski, and Ritchie [4], it has been known that the energy loss of the pair is not given by twice that of the individual proton. This nonlinearity arises from the so-called vicinage effect, where the stopping power for the pair of protons differs from twice the stopping power for individual protons due to the superposition of wake potentials induced by both fragments. Following that study, several experimental and theoretical studies have been performed [5–18]. In the theoretical studies, the vicinage effect has been treated as a result of interference in excitations of the target due to the closeness of the fragments. The interference occurs not only in collective plasmon excitation but also in the excitation of a single electron in the inner-shell orbital of a target atom and those excitations cannot be discerned experimentally [14–18].

At a glancing-angle incidence of a MeV H_2^+ ion to a single-crystal surface, the projectile dissociates to a pair of fragments at a few angstroms from the surface atomic plane. As the pair approaches the surface, the internuclear distance becomes large and the axis connecting the fragments becomes almost parallel to the surface [19,20]. The vicinage effect may be observed for the stopping power of the surface for the pair of fragments. The vicinage effect may depend on the internuclear vector between the fragments. The effect would also depend on the distance from the surface. Thus one may expect to study the dependence of the vicinage effect on the distance from the surface.

In this paper, the energy losses of the specularly reflected leading and trailing H^+ fragments at a glancing-angle incidence of (0.15–0.6)-MeV/amu H_2^+ ions on a clean SnTe(001) surface are measured at various angles of incidence less than 12 mrad. The energy losses are compared with those of H^+ ions at H^+ incidence with the same velocity. The energy losses are calculated using a classically obtained stopping power and approximated trajectories of fragments. From the calculated stopping power for a pair of fragments, the dependence of the vicinage effect not only on the internuclear distance but also on the distance from the surface atomic plane is discussed. The calculated energy losses are compared with the experimental ones.

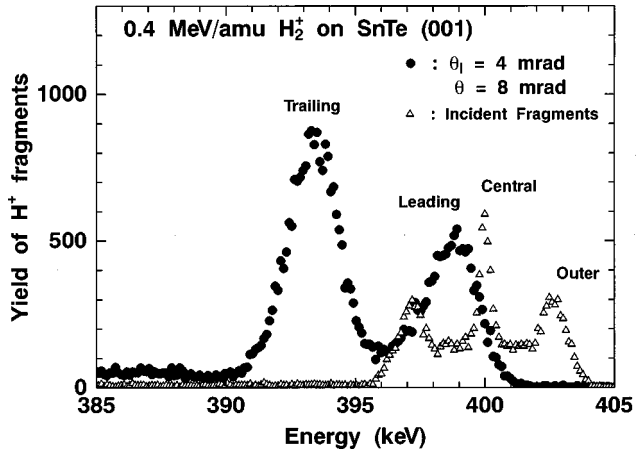

FIG. 1. Example of energy spectra of the H^+ fragments arising from dissociation of 0.4-MeV/amu H_2^+ ions at the SnTe(001) surface. The angle of incidence is 4 mrad and the angle of scattering is 8 mrad. The energy spectrum of the incident fragments arising from dissociation in collisions with residual gas molecules is also shown.

II. EXPERIMENTAL PROCEDURE

The main part of the experimental setup is described elsewhere [21,22], so the experimental procedures are briefly mentioned here. The (0.15–0.6)-MeV/amu H_2^+ ions from the 4-MV Van de Graaff accelerator of Kyoto University were collimated to have a maximal angular divergence of 0.1 mrad and be incident on a clean (001) surface of SnTe with glancing angles of incidence less than 12 mrad. The SnTe, which is a narrow-gap semiconductor of a NaCl-type crystal structure with a lattice constant 6.32 Å, is prepared by *in situ* evaporation on a KCl(001) surface under 10^{-10}-Torr ultrahigh vacuum conditions. The azimuthal angle of incidence was carefully adjusted in order to avoid surface channeling of the ions. The neutral fraction of the reflected fragments was less than 10^{-2}.

The energy spectra of H^+ fragments scattered in the scattering plane (the plane containing the incident beam direction and the target normal) at the angles for specular reflection, which are twice the angles of incidence, were measured by a 90° magnetic energy analyzer. The acceptance angle of the aperture placed before the analyzer was ± 0.1 mrad. The ion detector was a microchannel plate position-sensitive detector (PSD) and the position spectra on the PSD were collected in a multichannel analyzer. The energy resolution $\Delta E/E$ of the analyzer was about 10^{-3}. An anomalous electric signal from the PSD due to the simultaneous collision of two protons could not be found. This suggests that the observed fragments are singles of the pairs and that the angular deviation during the glancing-angle scattering is too large compared to the acceptance angle of the magnetic analyzer, ± 0.1 mrad, to detect both fragments of the pairs.

The energy losses of the fragments were determined by the shifts of the peak positions of the fragments in the energy spectra from that of the half energy of the incident H_2^+ ions, which was determined as follows. Having removed the target crystal from the beam and rotating the 90° analyzer to detect the incident beam of ions, the energy spectrum of incident ions was measured (an example of the energy spectrum is shown by triangles in Fig. 1). Three peaks of H^+ ions were observed in the energy spectrum, which were due to the H^+ fragments of H_2^+ formed by the dissociation in collisions with residual gas molecules in the beam transport. The three-peak structure is characteristic of the energy spectrum of fragments at H_2^+-gas collisions [23]. Although the yields of these peaks were negligibly small compared to that of the undissociated H_2^+ ions, the half energy of the incident H_2^+ ions was determined from the central peak of H^+ ions to avoid experimental error arising from tuning the magnetic field. In order to compare the energy loss of the fragments with that obtained at H^+-ion incidence, a similar experiment was performed at an incidence of (0.15–0.6)-MeV H^+ ions on the same surface.

III. EXPERIMENTAL RESULTS

An example of the energy spectra of H^+ fragments scattered from the surface of SnTe obtained at the 0.4-MeV/amu H_2^+-ion incidence is shown by closed circles in Fig. 1. Two peaks that correspond to the leading and trailing fragments are seen in the energy spectrum. The yield of the trailing H^+ fragments is larger than that of the leading H^+ fragments. This represents an effect of surface wake induced by the fragments [24]. In the energy spectrum of the incident fragments shown by triangles, three peaks are seen. The peak at 400 keV is the central peak and the other two peaks are the outer peaks arising from the collisions of H_2^+ projectiles with gases [23].

The energy losses of the leading and trailing fragments are obtained from the peak energies of the energy spectra of scattered fragments relative to that of the central peak of the incident fragments. The examples are shown in Fig. 2: Fig. 2(a) shows the energy losses for 0.2-MeV/amu ion incidence and Fig. 2(b) shows those for 0.4-MeV/amu ion incidence. For comparison, the energy losses of H^+ ions measured at H^+ incidence are also shown. These energy losses were measured a few times with different samples and averaged. The errors were estimated to be ± 0.2 keV, which may arise mainly from the measurements of the energies of the incident beams. It can be seen in Fig. 2 that the energy losses of the fragments do not depend so much on the angle of incidence. The independence is also observed for the energy losses of H^+ ions shown in the figures.

Figure 3 shows the sums of the energy losses of the leading and trailing H^+ fragments and the ratios of the sum of the energy losses of the fragments to twice the energy loss of individual H^+ ions. Figure 3(a) shows results for 0.2-MeV/amu ions and Fig. 3(b) for 0.4-MeV/amu ions. The sums of the energy losses of the fragments are about 1.05–1.15 times larger than twice the energy losses of the individual H^+ ions. The ratios are almost independent of the angle of incidence for both incidence energies. Figure 4 shows the incidence-energy dependence of the energy losses and the energy-loss ratios. The energy losses shown are averaged ones for a range of the angle of incidence, $(0.4 \pm 0.1)\theta_{cr}$, where θ_{cr} is the characteristic planar channeling angle for protons between (001) planes of SnTe [25]. The energy-loss ratios shown are taken between the averaged energy losses. The energy losses and ratios do not depend on the energy of incidence within the experimental errors.

The energy-loss differences between the leading and trail-

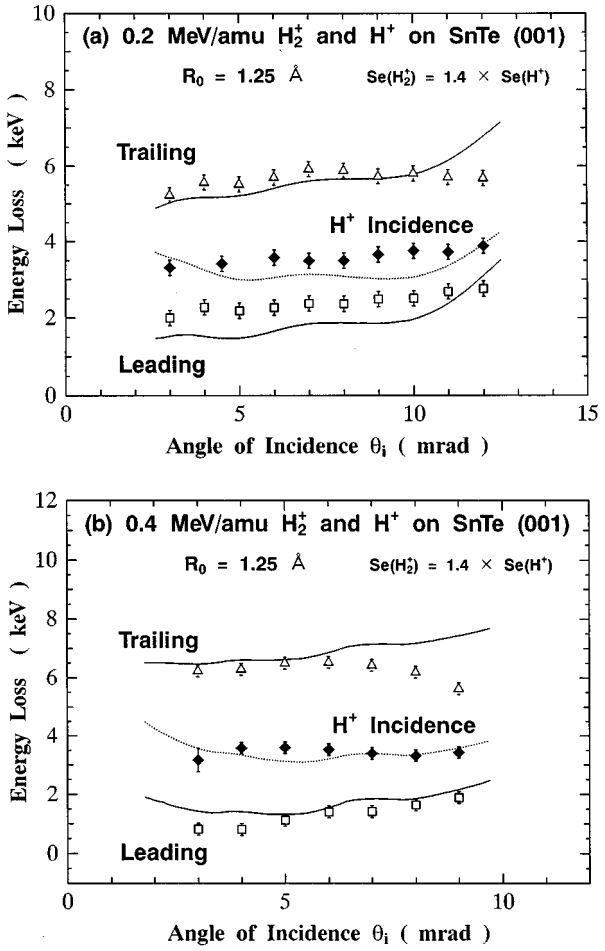

FIG. 2. Measured energy losses of the H^+ fragments as functions of the angle of incidence of projectiles. For comparison, the energy losses of H^+ ions at the incidence of individual H^+ ions are also shown. The lines are calculated energy losses for the individual, leading, and trailing H^+, where the square of the effective charge of H_2^+ ions is $z_{\rm eff}^2=1.4$. Results are shown for (a) 0.2-MeV/amu ions and (b) 0.4-MeV/amu ions.

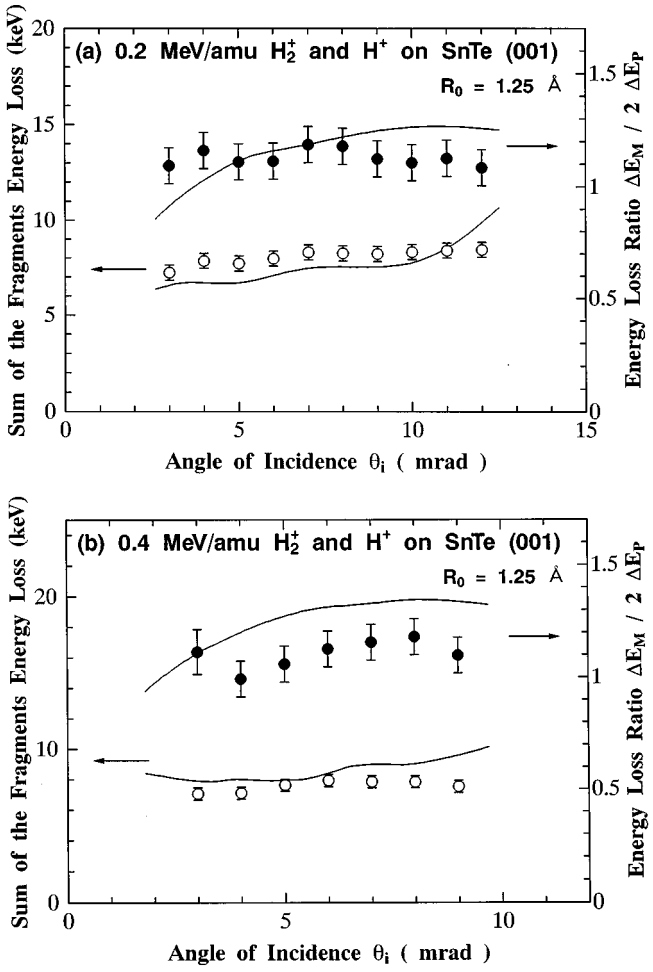

FIG. 3. Sum of energy losses of the leading and trailing fragments and their ratio to twice the energy loss of individual H^+ ions. The symbols are the experimental results and the lines are calculated ones, where the square of the effective charge of H_2^+ ions is $z_{\rm eff}^2=1.4$. Results are shown for (a) 0.2-MeV/amu ions and (b) 0.4-MeV/amu ions.

ing H^+ fragments [referred to as the energy separation $E_{\rm sep}(\theta_i)$ in the following] for the incidence of 0.2- and 0.4-MeV/amu H_2^+ ions are shown in Fig. 5. The energy separations are smaller than those calculated by Eq. (1) introducing $\Theta=0°$ and ν_c obtained by the Coulomb explosion in free space, which are shown in the figure by horizontal dotted lines. The reduction of the energy separations has been observed also for HeH^+ projectiles [20,24,26]. The incidence-energy dependence of the energy separation is shown in Fig. 6. The closed circles are the averaged data for the same range of the angle of incidence as in Fig. 4, where the energy separations for all the incidence energies investigated do not depend on the angle of incidence. The dotted curve is based on the same calculation as those shown in Fig. 5. The measured values are smaller than the calculated one.

IV. THEORETICAL STOPPING POWER OF SnTe(001) FOR A MeV PROTON

Before discussing the energy loss of a pair of protons resulting from the dissociation of H_2^+, the position-

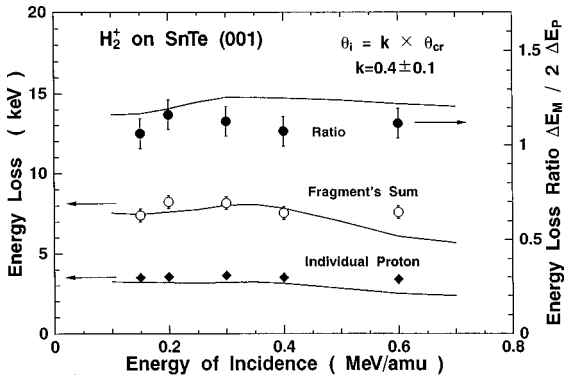

FIG. 4. Incidence-energy dependence of the sum of energy losses of the leading and trailing fragments and their ratio to twice the energy loss of individual H^+ ions. For comparison, the energy losses of H^+ ions at the incidence of individual H^+ ions are also shown. Symbols show experimental data averaged for the angle of incidence $0.3\theta_{\rm cr}<\theta_i<0.5\theta_{\rm cr}$ and lines show the calculated data averaged for the same region, where $\theta_{\rm cr}=7.65E_i^{-1/2}$ (mrad) and E_i is the incidence energy per proton of the projectiles in MeV.

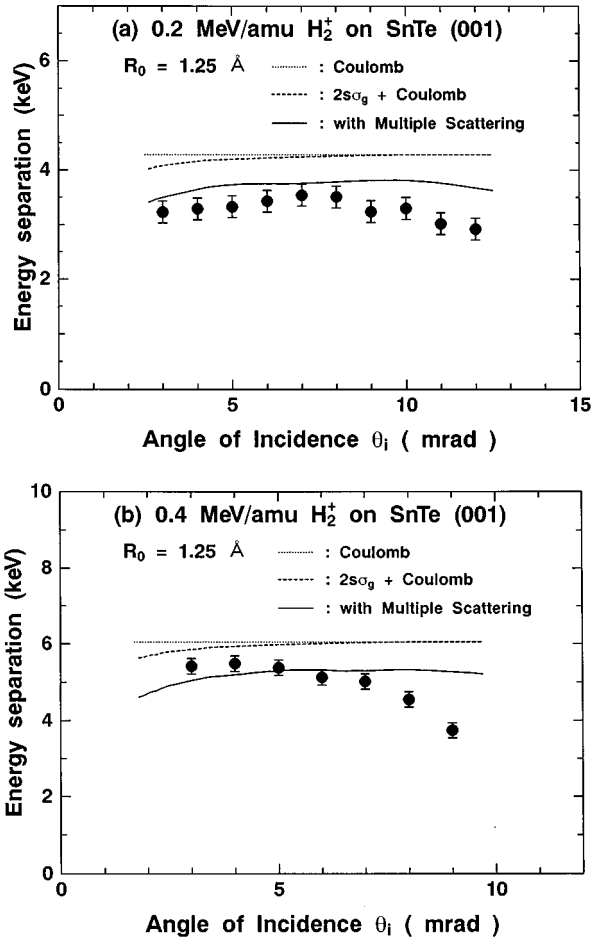

FIG. 5. Energy separation between the leading and trailing H^+ fragments. The closed symbols are the experimental data and the lines show the calculated data. The dotted line is for a free Coulomb explosion, the dashed line is obtained by the trajectory calculation using the $2s\sigma g$ state for the initial excitation, and the solid line is a result calculated by Eq. (23). In the calculation of Eq. (23), we have used $\nu_c(\theta_i)$ obtained from the dashed line and $\Delta E_P(\theta_i)$ obtained by the energy-loss calculation. Results are shown for (a) 0.2-MeV/amu H_2^+ ions and (b) 0.4-MeV/amu H_2^+ ions.

dependent stopping power for a specularly reflected MeV single proton at the (001) surface of SnTe is calculated. A Cartesian coordinate frame fixed with respect to the surface of crystal is considered, where the xy plane is parallel to the surface and the z axis is parallel to the surface normal. The total stopping power of the surface for a proton moving parallel to the surface at a distance from the surface atomic plane z is written as

$$S_P(z)=S_P^s(z)+S_P^c(z)\,, \tag{2}$$

where $S_P^s(z)$ is the stopping power for a proton due to single-electron excitation of a target atom and $S_P^c(z)$ is that due to collective excitation of the surface electrons.

The stopping power due to single-electron excitation is calculated by the following method by Basbas and Ritchie [16]. First, the collision of a proton moving with velocity $\vec{V}$ parallel to the x axis and a single-electron atom is considered, where the electron is harmonically bound to the

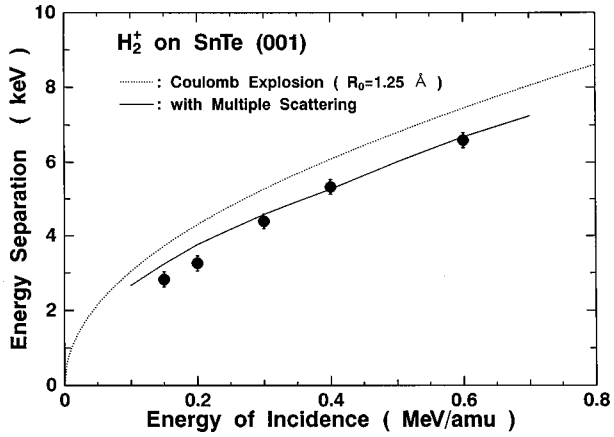

FIG. 6. Incidence-energy dependence of the energy separation. Symbols show experimental data averaged for the angle of incidence $0.3\theta_{cr}\leqslant\theta_i\leqslant 0.5\theta_{cr}$. The dotted line is calculated for a free Coulomb explosion and the solid line is calculated using Eq. (23), which is averaged for the same region of the angle of incidence.

nucleus. Assume that the proton is deflected only slightly in the collision. The equation of motion of the electron is given by

$$m\,\frac{d^2\vec{r}}{dt^2}+m\omega^2\vec{r}=\nabla_{\vec{r}}\left[\frac{e^2}{|\vec{r}-\vec{V}t-\vec{b}|}\right], \tag{3}$$

where m is the electron mass, $\vec{b}$ is the impact parameter of the collision, and the electron is bound to the nucleus with angular frequency ω. When b is larger than r, the variation of the electric field on the position of the electron may be neglected and the energy transfer from the proton to the atom after the collision is obtained as [27]

$$\delta E_P(b)=\frac{e^4}{2m}\left|\int_{-\infty}^{\infty}dt\;e^{i\omega t}\left[\nabla_{\vec{r}}\,\frac{1}{|\vec{r}-\vec{V}t-\vec{b}|}\right]_{\vec{r}\to 0}\right|^2$$

$$=\frac{e^4}{2\pi^2 mV^2}\left|\int\frac{\vec{q}\;d^2\vec{Q}}{q^2}\,e^{-i\vec{Q}\cdot\vec{b}}\right|^2, \tag{4}$$

where $\vec{q}=\omega/V\hat{x}+\vec{Q}$, $\hat{x}$ is the unit vector along the x axis, and $\vec{Q}$ is the wave-vector transfer in the yz plane. According to Basbas and Ritchie, the upper limit of the integration with respect to $\vec{Q}$ in Eq. (4) is

$$|\vec{Q}_m(\omega)|=\sqrt{k_{\max}^2-\omega^2/V^2},\quad k_{\max}=2mV/\hbar. \tag{5}$$

They integrated the $\delta E_P(b)$ term of Eq. (4) over $\vec{b}$ and $\vec{Q}$ and obtained the stopping cross section of the electron for a proton. Since the impact-parameter dependence of the energy transfer is needed to carry out this work, integration of the energy transfer in Eq. (4) over $\vec{Q}$ only is carried out as

$$\delta E_P(\omega;b)=\frac{2e^4}{mV^2}\left[\frac{\omega^2}{V^2}\left(\int_0^{Q_m(\omega)}\frac{dQ\ Q\ J_0(Qb)}{Q^2+\omega^2/V^2}\right)^2+\left(\int_0^{Q_m(\omega)}\frac{dQ\ Q^2 J_1(Qb)}{Q^2+\omega^2/V^2}\right)^2\right], \tag{6}$$

where J_0 and J_1 are the zeroth- and first-order Bessel function of the first kind. The right-hand side of Eq. (6) is a function of ω; thus $\delta E_P(b)$ is denoted by $\delta E_P(\omega;b)$ in the following.

This atomic model is generalized to one consisting of $Z^{(A)}$ harmonically bound electrons with the ith electron having oscillator strength f_i and resonant frequency ω_i. Since the electrons in the atom are assumed to be mutually independent, harmonically bound classical electrons, f_i may be set equal to unity [28]. Then introducing n_j, which is the number of electrons having the resonant frequency ω_j in the jth shell, and the oscillator strength $f_j=n_j/Z^{(A)}$ corresponding to this transition, the energy transfer expressed by Eq. (6) can be written by

$$\delta E_P^{(A)}(b)=Z^{(A)}\sum_j f_j\delta E_P(\omega_j;b), \tag{7}$$

where the superscript (A) denotes the atomic species and the summation is carried out for electronic shells where the electrons can be excited, i.e., $k_{\max}^2\geqslant\omega_j^2/V^2$.

Now consider a surface of a single crystal that is parallel to the xy plane. For a proton moving parallel to the x axis over the surface, the energy loss per unit path length due to single-electron excitations of the surface atoms is defined by

$$S_P^s(z)=\sum_A N^{(A)}\int_{-\infty}^{\infty}\delta E_P^{(A)}(b)dy, \tag{8}$$

where $N^{(A)}$ is the areal density of A atomic species on the surface and $b=(y^2+z^2)^{1/2}$.

The stopping power due to the collective excitation of valence electrons for a proton moving at a distance $z=z_0$ from the surface atomic plane is given by

$$S_P^c(z)=e\left.\frac{\partial U_P(\vec{r},z_0)}{\partial x}\right|_{x=0,y=0,z=z_0}, \tag{9}$$

where $U_P(\vec{r},z_0)$ is the surface-wake potential induced by the proton moving at $(0,0,z_0)$ parallel to the surface of a semi-infinite homogeneous medium [29,30]. The analytical formula for $U_P(\vec{r},z_0)$ is expressed in Ref. [24]. Substituting the formula shown in Ref. [24] into Eq. (9), the stopping power of the surface due to the collective excitation for a proton moving at a distance z from the surface atomic plane is obtained as

$$S_P^c(z)=\frac{\omega_s^2e^2}{V^2}\int_0^{V/\nu_F}\frac{\zeta J_0\left(\frac{\omega_s}{V}\zeta 2|z'|\right)}{1+\zeta^2}d\zeta+\left[\frac{\omega_p^2e^2}{V^2}\int_0^{V/\nu_F}\frac{\zeta\left[1-J_0\left(\frac{\omega_p}{V}\zeta 2|z'|\right)\right]}{1+\zeta^2}d\zeta\right]\times\Theta(-z'), \tag{10}$$

where the distances z' and z_0' are measured from the surface of a semi-infinite homogeneous medium, ω_p and ω_s are the bulk- and surface-plasma angular frequencies, ν_F is the Fermi velocity of solid electrons, and $\Theta(-z')$ is the unit step function, which shows that the second term is needed when the proton is inside the surface.

In the calculation of Eq. (8), ω_j was approximated by $\omega_j=I_j/\hbar'$, where I_j is the ionization energy of the jth shell electrons of the Sn and Te atoms [31]. The choice of the surface of a semi-infinite medium at 0.5 monolayer (ML) (1.58 Å) outside the center of the (001) atomic plane of the surface of SnTe has been succeeded in explaining the energy loss of specularly reflected ions [32]. The plasmon frequencies ω_s and ω_p and the Fermi velocity ν_F of SnTe, calculated from the density of valence ($5s$ and $5p$ shells) electrons of five electrons per atom, agree with experimental data [33,34] and have been successful in the analysis of dissociation [24]. With these parameters and the use of Eqs. (2), (8), and (10), the total stopping power $S_p(z)$ of the (001) surface of SnTe is calculated.

The results of the calculation for a 0.2-MeV proton are shown in Fig. 7 as functions of the distance from the surface atomic plane, where the stopping power due to single-electron excitation, that due to the collective excitation, and the total stopping power are shown. The stopping power due to single-electron excitations has an oscillatory structure, which is due to the oscillation of the Bessel functions in the energy transfer expressed by Eq. (6), and its period is mainly determined by $Q_m(\omega_j)$. Since the $Q_m(\omega_j)$'s do not depend so much on the shells (e.g., 10.2 Å^{-1} for $4s$-shell electrons and 10.7 Å^{-1} for $5p$-shell electrons in the Sn atom), the oscillation in the energy transfer is not smeared by the summation over shells. The stopping power due to single-electron excitation becomes smaller with the increasing distance from the surface, while the stopping power due to collective excitation becomes dominant as the distance becomes large. The experimental stopping power shown in Fig. 7 was obtained from the measured incidence-angle dependence of the energy loss of protons with the use of the analysis reported in Ref. [32]. It can be seen that the theoretically obtained total stopping power agrees with the experimental one within a factor about 2.

The calculated energy loss of an individual proton obtained by the integration of the stopping power along trajectories of protons scattering at glancing-angle incidence on the surface is shown in Fig. 2. Here the trajectory of the proton is calculated under the surface continuum potential derived from the Molière approximation for the screening function of Thomas-Fermi type. The experimental results for the individual proton are fairly reproduced by the calculation

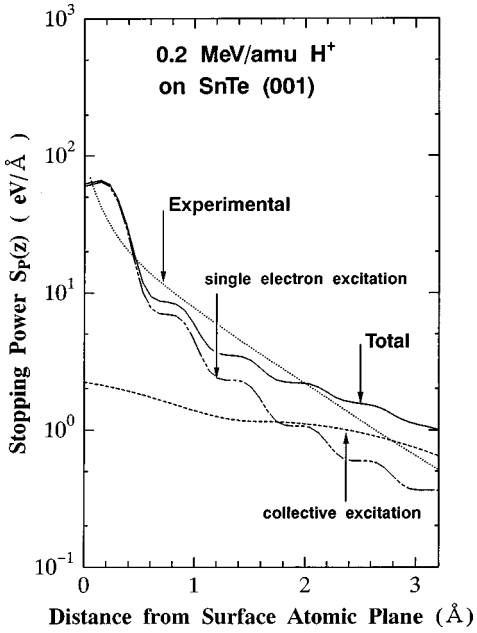

FIG. 7. Calculated results for stopping powers for 0.2-MeV proton as functions of the distance from the surface atomic plane. The ionization energies of the Sn atom used in the calculation are 9.761, 7.060, 2.5262, 0.9192, and 0.4370 Ry for $4s$, $4p$, $4d$, $5s$, and $5p$ electrons, respectively. The ionization energies of Te atom used are 11.899, 8.921, 3.8208, 1.2594, and 0.6328 Ry for $4s$, $4p$, $4d$, $5s$, and $5p$ electrons, respectively. The areal density of the target Sn and Te atoms, $N^{(\mathrm{Sn})}=N^{(\mathrm{Te})}=N$, is 0.0504 Å^{-2}, the bulk and surface plasma angular frequencies are 2.19×10^{16} and 1.55×10^{16} sec^{-1}, respectively, and the Fermi velocity $\nu_F=1.89\times10^6$ m/s. For comparison, the stopping power obtained from experimental energy-loss data for 0.2-MeV protons is also shown.

for both energies of incidence. The maximal deviation between the calculated and experimental results is about 20%.

The calculated incidence-energy dependence of the energy loss of a proton is shown in Fig. 4, which is averaged in the same region of the angle of incidence as the experimental one. The agreement between the calculated energy loss and the experimental one is good at an incidence energy less than 0.4 MeV/amu. However, the calculated energy loss decreases as the energy of incidence becomes larger than 0.5 MeV/amu. This decrease is related to the explicit velocity dependence of the energy transfer described by Eq. (6) and the atomic shells of electrons, which can be excited as in Eq. (7).

V. THEORETICAL STOPPING POWER OF SnTe(001) FOR A PAIR OF MeV PROTONS

Although we have not been successful in detecting well-aligned pairs with the beam direction in the present experimental conditions, where fragments scattered only at the angle for specular reflection are measured, our theoretical treatment is only for the pair whose internuclear vector is aligned with the beam direction. This treatment is based on two assumptions: The first is that the fragments measured at $\theta=2\theta_i$ arise from pairs whose internuclear vectors are parallel to the surface, where θ is the scattering angle measured in the xz plane perpendicular to the surface. The second is that the fragments measured at $\phi=0°$ arise from pairs whose internuclear vectors are in the xz plane, where ϕ is the scattering angle measured in a plane parallel to the surface. A discussion concerning these assumptions will be carried out in Secs. VII and VIII A.

In analogy with Eq. (2), the total stopping power for a pair of protons moving parallel to the surface at the distance from the surface, with the internuclear distance R, is written as

$$S_M(R,z)=S_M^s(R,z)+S_M^c(R,z), \tag{11}$$

where $S_M^s(R,z)$ is the stopping power for a pair of protons due to the single-electron excitation of a target atom and $S_M^c(R,z)$ is that due to the collective excitation of the surface electrons. The stopping power for a pair of protons due to single-electron excitation is also calculated by the theory of Basbas and Ritchie [16]. At the collision of a pair of protons aligned with the beam direction and a one-electron atom introduced in Sec. IV, the equation of motion of the electron must contain an additional term $e^2/|\vec{r}-\vec{V}t-\vec{b}-R\hat{x}|$ on the right-hand side of Eq. (3). The energy transfer to the atom from the pair of protons becomes

$$\delta E_M(\omega;R,b)=2\left[1+\cos\left(\frac{\omega R}{V}\right)\right]\delta E_P(\omega;b), \tag{12}$$

where $\delta E_P(\omega;b)$ is the energy transfer from a proton to the atom given by Eq. (6). The energy transfer $\delta E_M(\omega;R,b)$ from the pair of protons at the collision with the atom consisting of $Z^{(A)}$ harmonically bound electrons is

$$\delta E_M^{(A)}(R,b)=2Z^{(A)}\sum_j f_j\left[1+\cos\left(\frac{\omega_j R}{V}\right)\right]\delta E_P(\omega_j;b). \tag{13}$$

Thus the stopping power of a surface plane for a pair of aligned protons moving parallel to the x axis due to the excitation of a single electron is

$$S_M^s(R,z)=\sum_A N^{(A)}\int_{-\infty}^{\infty}\delta E_M^{(A)}(R,b)\,dy. \tag{14}$$

The stopping power due to the collective excitation of valence electrons at the surface for the pair of protons moving at a distance $z=z_0$ from the surface atomic plane is given by

$$\begin{aligned} S_M^c(R,z)&=e\left.\frac{\partial U(\vec{r},z_0)}{\partial x}\right|_{x=0,y=0,z=z_0} \\ &\quad+e\left.\frac{\partial U(\vec{r},z_0)}{\partial x}\right|_{x=R,y=0,z=z_0}, \\ U(\vec{r},z_0)&=U_P(\vec{r},z_0)+U_P(\vec{r}-R\hat{x},z_0). \end{aligned} \tag{15}$$

Substituting the formula for the wake potential into Eq. (15), the contribution due to the collective excitation to the stopping power for the pair of protons moving at a distance z_0 from the surface atomic plane is obtained as

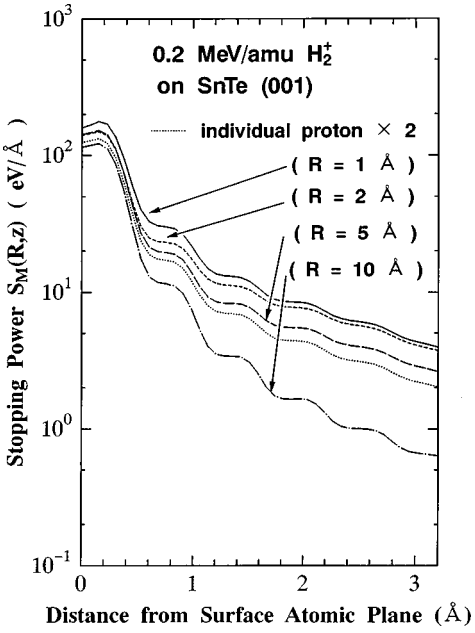

FIG. 8. Stopping powers for a pair of the leading and trailing protons with internuclear distances of 1, 2, 5, and 10 Å for an incidence of 0.2-MeV/amu H_2^+ ions. For comparison, twice the stopping power for an individual proton is also shown.

$$S_M^c(R,z)=2\left[1+\cos\left(\frac{\omega_s R}{V}\right)\right]\frac{\omega_s^2 e^2}{V^2}\times\int_0^{V/\nu_F}\frac{\zeta J_0\left(\frac{\omega_s}{V}\,\zeta 2|z'|\right)}{1+\zeta^2}d\zeta+2\left[1+\cos\left(\frac{\omega_p R}{V}\right)\right]\frac{\omega_p^2 e^2}{V^2}\times\int_0^{V/\nu_F}\frac{\zeta\left[1-J_0\left(\frac{\omega_p}{V}\,\zeta 2|z'|\right)\right]}{1+\zeta^2}\,d\zeta\;\Theta(-z'). \tag{16}$$

With the parameters used in Sec. IV, Eqs. (14) and (16) are calculated and the total stopping power for a pair of aligned protons $S_M(R,z)$ is obtained in Eq. (11). It must be noted from Eqs. (14) and (16) that $S_M(R,z)=4S_P(z)$ when $R=0$. However, $S_M(R,z)$ does not approach $2S_P(z)$ at $R=\infty$ because no damping mechanism is introduced in this model.

Figure 8 shows the total stopping powers calculated for a pair of protons aligned with the beam direction with internuclear distances of 1, 2, 5, and 10 Å. For comparison, twice the total stopping power for the individual proton is also shown. The stopping powers for the pair of fragments are different from twice the stopping power for an individual proton. The difference depends on the internuclear distance of the pair of protons and on the distance from the surface, where the difference decreases as the distance from the surface decreases.

The dependence of the ratio of the stopping powers for a pair of protons to that for an individual proton on the internuclear distance (R) and the distance from the surface (z) is shown in Fig. 9. The contour map of the ratio in the Rz plane is also shown at the bottom of the figure. At a distance from the surface larger than 2 Å in Fig. 9, the ratio monotonically oscillates along the R axis. Here the stopping powers due to excitations of the surface wake and electrons in the $5s$ and $5p$ shells of Sn and Te atoms are dominant. The oscillation corresponds to superposition of $\cos(\omega_j R/V)$ in Eq. (13) for the $5s$ and $5p$ electrons and $\cos(\omega_s R/V)$ in Eq. (16). The wavelength of the resultant oscillation is close to the wavelength of the surface wake, $2\pi V/\omega_s$, which is 24 Å for 0.2-MeV/amu ions. At a distance from the surface smaller than 1 Å, the ratio has a complicated oscillatory structure around unity. Here the stopping power is mostly determined by the excitations of the $4s$, $4p$, and $4d$ electrons of Sn and Te atoms. The oscillation of the ratio corresponds to the superposition of $\cos(\omega_j R/V)$ for these excitations. Because the frequencies for these excitations are large compared to those for surface plasmon excitations, the wavelength of the oscillations is small compared to that of the surface wake.

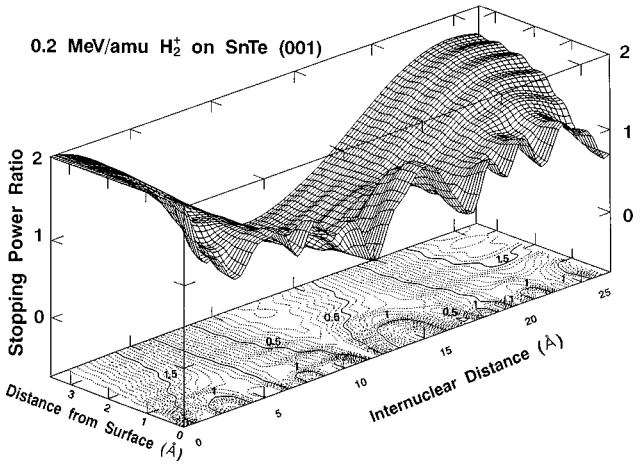

FIG. 9. Ratio of the calculated stopping powers for a pair of protons to twice that of the individual proton as a function of the internuclear distance between them and their distance from the surface atomic plane. The energy of incidence of the projectiles is 0.2 MeV/amu.

VI. ENERGY LOSSES OF REFLECTED FRAGMENTS AT MeV H_2^+ INCIDENCE

A. Dissociation of H_2^+ during glancing-angle scattering

The energy loss of a pair of fragments is calculated by integrating the stopping power along the ion trajectory whose initial internuclear distance R_0 was assumed to be 1.25 Å [35]. Thus a model for the trajectory, which gives the internuclear distance as a function of the distance from the surface, is needed for the calculation of the energy losses. Here the trajectories of the pairs of fragments aligned with the beam direction are approximated. The procedure of the trajectory calculation, which revises the trajectory simulation for the MeV HeH^+ incidence shown in Ref. [26], is as follows.

Assume that the center of mass of H_2^+ is on a trajectory $z(x)$, which is defined by the angle of incidence of H_2^+ to the surface and the surface continuum potential described by the Molière approximation for the screening function of

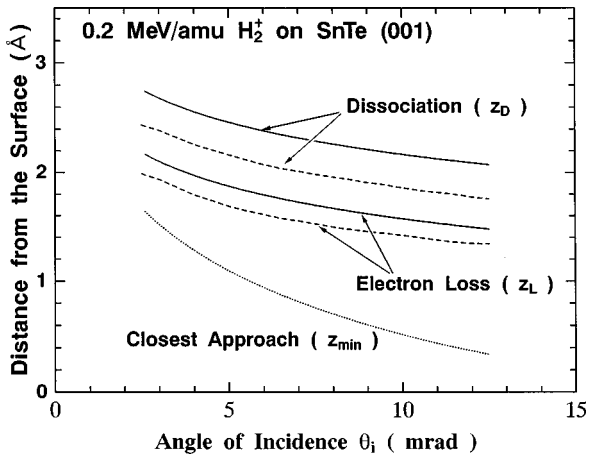

FIG. 10. Distances from the surface atomic plane where the dissociation of H_2^+ and the ionization of H^0 fragments take place for an incidence of 0.2-MeV/amu H_2^+ ions. The solid lines show the results calculated from electron density distributions obtained from the Molière approximation of the Thomas-Fermi potential, where the Thomas-Fermi screening radius for the proton-SnTe collision is 0.126 Å, and the dotted lines show the results from the electron distributions obtained by the Hartree-Fock calculation of single Sn and Te atoms. The closest approach to the surface atomic plane is also shown for comparison.

Thomas-Fermi type. The dissociation of H_2^+ into H^+ and H^0 occurs by the excitation that is caused by the collisions of the projectile with electrons at the surface. The survival probability $P_s(z)$ of the H_2^+ ions in collisions with the electrons is given by

$$P_s(z)=\exp\left(-\sigma_D\int_{\text{traj: } x=-\infty}^{z(x)} n(z)ds\right), \tag{17}$$

where the curvilinear integral is performed along the trajectory $z(x)$, σ_D is the dissociation cross section of H_2^+, and $n(z)$ is the electron density outside the surface atomic plane, which is calculated from the surface continuum potential. For convenience of the following calculation, it is assumed that all H_2^+ ions dissociate into H^+ and H^0 when the exponent of Eq. (17) is -1. Thus the position $z_D(x_D)$ of dissociation of H_2^+ is defined by

$$\sigma_D\int_{\text{traj: } x=-\infty}^{z_D(x_D)} n(z)ds=1. \tag{18}$$

The position $z_L(x_L)$ for ionization of H^0 fragments is determined by the same procedure as

$$\sigma_L\int_{\text{traj: } z=z_D}^{z_L(x_L)} n(z)ds=1, \tag{19}$$

where the integration is along the trajectory and σ_L is the electron-loss cross section of H^0 at the collisions with electrons.

For the dissociation cross section σ_D, the proton production cross section measured at the electron impact on H_2^+ with the collision velocities equal to the present experiment is chosen [36]. Similarly, for σ_L, the electron-loss cross section for H^0 is chosen [37].

The distances from the surface obtained, where the excitation of H_2^+ and electron loss of H^0 fragments take place, are shown in Fig. 10 for the incidence of 0.2-MeV/amu H_2^+ ions. Both distances slightly decrease as the angle of incidence increases. The distances are comparable to our earlier estimates [19,20,24,26] and they are comparable to the distance from the surface where the charge-exchange collisions occur frequently [38]. The fragments approach the surface atomic plane and are repelled from the surface, repelling each other due to the interaction potential of the excited state when one of the fragments is H^0 and due to the bare Coulomb potential when both fragments are H^+. The closest approach is shown in Fig. 10 for a comparison with the distances for dissociation and ionization.

B. Energy loss of a pair of aligned fragments

The energy loss of a pair of fragments is calculated by integrating the stopping power for the fragments along the trajectory of the pair as

$$\Delta E_M=z_{\text{eff}}^2\left[\int_{\text{traj: } x=-\infty}^{z_D} S_p(z)ds+\int_{\text{traj: } z=z_D}^{z_L} S_p(z)ds\right]+\int_{\text{traj: } z=z_L}^{x=\infty} S_M(r,z)ds \tag{20}$$

where z_{eff}^2 is the square of the effective charge of the molecular H_2^+ ions and the stopping powers for the H_2^+ ions in the ground state and excited states are approximated by $z_{\text{eff}}^2 S_p(z)$. Since the stopping powers shown in Fig. 8 become larger as the distance from the surface decreases and the electron loss of the H^0 fragments occurs at larger distances compared to the closest approaches to the surface as shown in Fig. 10, the stopping powers for the molecular ions contribute only less than 10% of the total energy loss. For the square of the effective charge of the ground-state H_2^+ ions, one experimental datum for 9.6-MeV/amu H_2^+ ions in carbon foils [39] and a theoretical prediction by Kaneko for H_2^+ ions in our energy region [17] can be referred. The measured square of the effective charge for H_2^+ ions in carbon foils and calculated ones for carbon, Al, and Kr targets were compiled to be 1.4 ± 0.1 [17,39]. Thus $z_{\text{eff}}^2=1.4$ is used in the present calculation.

The calculated results for the energy losses of a pair of fragments are shown in Fig. 3. Although the internuclear distance at the surface depends slightly on the excited state selected (e.g., the $2s\sigma_g$ or $2p\sigma_u$ states), the resulting difference in the energy losses is negligible. The results shown are calculated using the $2s\sigma_g$ state for the excited state. The agreement between the measured sums of the energy losses and the theoretical sums for the pair of protons is good for both incidence energies. The maximal deviation between the calculated and experimental results is about 15%, except at the largest angles of incidence. The calculated energy-loss ratios are also shown in Fig. 3. The calculated ratio agrees well with the experimental one for 0.2-MeV/amu ions, but is slightly larger than the experimental one for 0.4-MeV/amu ions.

Figure 4 shows the calculated incidence-energy dependence of the energy loss of a pair of protons and of the energy-loss ratio. The calculated results of the ratio are al-

most independent of the energy of incidence. The independence is consistent with, but slightly larger than, experimental results.

VII. CORRECTION OF MULTIPLE SMALL-ANGLE SCATTERING

The energy-loss differences between the leading and trailing fragments shown in Figs. 5 and 6 are smaller than those calculated by Eq. (1) introducing $\Theta=0°$ and ν_c obtained by the Coulomb explosion in free space. Shown in Fig. 5 are the energy separations obtained by the present trajectory calculation using the $2s\sigma_g$ state for the initial excitation of H_2^+ ions. Although the calculated energy separations slightly depend on the angle of incidence, they are nearly equal to the Coulomb value. This shows that the calculated energy separation does not depend on the initial excited states. Thus the experimental energy separation cannot be explained by the choice of the states [26].

For the trajectory simulation of the glancing-angle incidence of MeV HeH^+ on SnTe shown in Refs. [20, 26], the calculated distributions of H^+ fragments are convoluted with a three-dimensional Gaussian distribution in θ, ϕ, and E in order to take into account the multiple scattering and the energy resolution of the analyzer. For H_2^+ projectiles, since the angular spread by the Coulomb explosion is comparable to the full width at half maximum (3–5 mrad) of the angular distribution of fragments caused by multiple small-angle scattering, the multiple scattering can reduce the energy separation. In this work, the energy separation taking into account the multiple scattering is calculated as follows.

(i) The internuclear vectors connecting the exploding fragments become parallel to the surface due to the effect of the surface continuum potential [19]. Roughly, all of the fragments detected at the angle for specular reflection are assumed to arise from pairs whose internuclear vectors become parallel to the surface after the dissociation starts. Thus, before taking into account the multiple scattering, the change of c.m. velocity of fragments perpendicular to the surface is neglected and only the c.m. velocity parallel to the surface is considered. The components parallel and perpendicular to the beam direction of the c.m. velocity acquired by fragments can be written as $\nu_c(\theta_i)\cos\phi_0$ and $\nu_c(\theta_i)\sin\phi_0$, respectively, where $\nu_c(\theta_i)$ is the c.m. velocity of a fragment acquired by dissociation and ϕ_0 is the angle between the molecular axis and incident beam direction measured in the plane parallel to the surface [20,24,26].

(ii) The scattering angle θ and ϕ distributions are smeared by Gaussian distribution due to the multiple scattering. Applying the impulse approximation and neglecting the scattering geometry concerning the surface to calculate the standard deviation of the Gaussian distribution, the standard deviation is given by

$$\sigma(\theta_i)=\sqrt{\frac{m\Delta E_P(\theta_i)}{M_p E_i}}, \tag{21}$$

where $\Delta E_P(\theta_i)$ is the energy loss of a proton and E_i is the incidence energy per proton. Here the correlation of the two fragments during the scattering is also neglected since it is expected to be a minor effect [40–42].

(iii) The detection probability of the fragments arising from H_2^+ ions whose molecular axes are tilted by an angle ϕ_0 with respect to the incident beam direction is given by

$$P(\theta_i,\phi_0)=\frac{1}{\pi\, V^2\sigma(\theta_i)^2}\int_0^{V\theta_W} V_\rho dV_\rho \int_0^{2\pi} d\xi \times\exp\left[-\frac{[\nu_c(\theta_i)\sin\phi_0+V_\rho\cos\xi]^2+[V_\rho\sin\xi]^2}{V^2\sigma(\theta_i)^2}\right], \tag{22}$$

where θ_W is the experimental detection angle, which is 0.1 mrad, V_ρ is the velocity of fragments perpendicular to the incident beam direction acquired by the multiple scattering, and ξ is the angle between V_ρ and the crystal surface. Here the asymptotic c.m. velocity of the fragment acquired by the dissociation is treated as a function of θ_i.

(iv) The final mean energy separation can be written as

$$E_{\rm sep}(\theta_i)=2M_pV\nu_c(\theta_i)\int_0^{\pi/2} D(\phi_0)P(\theta_i,\phi_0)\cos\phi_0 d\phi_0, \tag{23}$$

$$D(\phi_0)d\phi_0=\frac{2}{\pi}d\phi_0,$$

where $D(\phi_0)$ is the initial distribution function of the pair whose angle of the axis with respect to the incident beam direction is between ϕ_0 and $\phi_0+d\phi_0$.

The calculated energy separations for 0.2- and 0.4-MeV/amu H_2^+-ion incidence are shown in Fig. 5. The agreements between the experimental and calculated results are good, except at the angles of incidence larger than 8 mrad for 0.4-MeV/amu H_2^+ ions, where the multiple scattering due to collisions with thermally vibrating atoms cannot be neglected [43].

The calculated ϕ_0 distribution of the pair whose one fragment is detected at the angle for specular reflection, i.e., $D(\phi_0)P(\theta_i,\phi_0)d\phi_0$, is not sharply peaked at $\phi_0=0°$. However, it was found from the calculation that more than half of the detected fragments arise from $\phi_0<15°$. Applying the stopping power for aligned pairs, the energy losses of the leading and trailing fragments can be written as

$$\Delta E_L(\theta_i)=\frac{\Delta E_M(\theta_i)-E_{\rm sep}(\theta_i)}{2},$$
$$\Delta E_T(\theta_i)=\frac{\Delta E_M(\theta_i)+E_{\rm sep}(\theta_i)}{2}, \tag{24}$$

respectively. The energy losses are shown in Fig. 2. The agreement between the calculated and experimental energy losses of fragments is fairly good.

VIII. DISCUSSION

A. Calculated energy losses

The maximal deviation between the calculated and the experimental energy loss for protons is about 20%, as shown in Fig. 2. For the stopping power for a pair of fragments, the approximations made in the stopping power may cause an error as large as that for a proton. Further, several approximations on the trajectories of a pair of fragments may also

cause error in the energy loss of a pair of fragments. Discussions concerning the reliability of the calculations and errors arising from changing the parameters used are made in the following.

The stopping power due to the single-electron excitation of the target atom used in this model is based on Bohr's harmonic-oscillator model. In this study, not all possible excitations are treated. That is, each electron of the target atom is approximated by a harmonically bound electron with only one resonant frequency ω_j for ionization and $\cos(\omega_j R/V)$ terms in Eq. (13) superposed at a distance from the surface z smaller than 1 Å. If ω_j's for all possible excitations of the target atom are introduced and cosine terms corresponding to these excitations are summed over, the structure of the ratio may change at a small distance from the surface, where the single-electron excitation is dominant. It is expected that the ratio approaches unity by the superposition of many cosine terms, except for the cases where many ω_j are harmonic or only a few cosine terms are strongly weighted. The present choice of one-fixed resonant frequency ω_j may cause considerable error in the stopping power for a pair of fragments and in the stopping power ratio at the small distance from the surface.

The stopping power due to collective excitation of the surface electrons is expressed by a formula for the surface-wake potential induced by a proton moving parallel to the surface of a semi-infinite homogeneous medium. Arista has shown that the results of the stopping power calculated for an ideal free-electron gas may give erroneous results in many cases [44]. A comparison of the stopping power for 0.2-MeV protons shown in Fig. 7 with that obtained by the formula derived by Kitagawa with the use of a dielectric function for an inhomogeneous electron gas under the local-density approximation [32,45] has been made. For $z>2.5$ Å, where the relative contribution to the stopping power from the collective excitation is large, the stopping powers agree well with each other. Thus the assumption of the homogeneous medium may not give a serious error for this work.

In the present calculation, the distances from the surface for dissociation and ionization are derived from the electron density obtained by the Molière approximation for the screening function of Thomas-Fermi type. The Molière approximation is useful in the description of the elastic scattering of high-energy ions by target atoms. The approximation is of simple analytical form and tends to come closer to the Hartree value at large distances [25]. Thus the present electron distribution on the SnTe surface for $0.5\ \text{Å} \leqslant z \leqslant 5$ Å is not different by a factor 2 from that obtained by summation of the Hartree-Fock calculation for isolated Sn and Te atoms [31]. The distances from the surface for dissociation and ionization using the electron density obtained by the Hartree-Fock calculation are also shown in Fig. 10. These distances are small compared to those used in the present calculation. The differences in the distances contribute less than 2% to the final energy loss. The energy loss of a pair of fragments and the energy-loss ratio calculated using the electron density obtained by the Hartree-Fock calculation are shown in Fig. 11(a) and are compared with the results shown in Fig. 3(a).

In the present calculation, the stopping powers for the ground-state and excited-state H_2^+ ions are unknown parameters. The assumed stopping power for the molecular ions affects $\pm 7\%$ of the total energy loss for $1 \leqslant z_{\text{eff}}^2 \leqslant 2$. The energy losses of a pair of fragments and the energy-loss ratios calculated by using $z_{\text{eff}}^2=1$ and 2 are shown in Fig. 11(b)

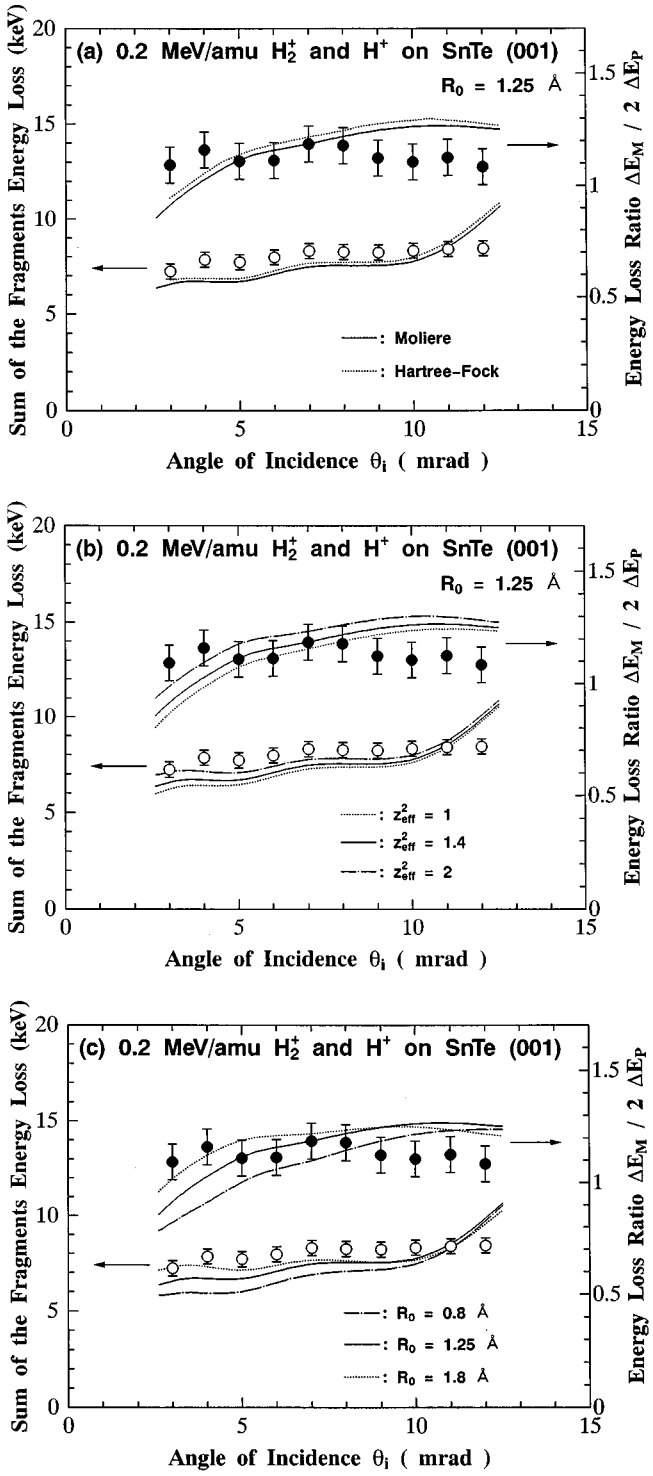

FIG. 11. Comparison of the calculated energy loss of a pair of fragments and the energy-loss ratio with those obtained in other conditions: (a) comparison with the results calculated using the electron density obtained by Hartree-Fock calculations, (b) comparison with the results calculated using $z_{\text{eff}}^2=1$ and 2, and (c) comparison with the results calculated by using initial internuclear distance $R_0=0.8$ and 1.8 Å.

and are compared with the results shown in Fig. 3(a).

The calculated results would also depend on the distribution of the internuclear distance of H_2^+ in the incident beam. The calculated results shown in Fig. 3 are those for the mean value of the initial internuclear distance ($R_0 = 1.25$ Å). Most of the distribution is considered to be within $0.8\ \text{Å} \leq R_0 \leq 1.8\ \text{Å}$ [23]. The calculated results for initial internuclear distances of 0.8 and 1.8 Å are shown in Fig. 11(c). The differences in the energy loss are within 10%. Although the calculated results must be averaged by integrating after multiplying the distribution function of R_0, the averaged values are expected to be similar to the present values calculated using the mean value of R_0.

Our treatment is only for the pair whose internuclear vector is aligned with the beam direction, which depends on the assumptions described in Sec. V. These assumptions are based on our earlier experimental studies with computer simulations [19,20,24,26]. Tracing the trajectories of 0.2-MeV/amu fragments using a computer simulation [26], it is found that most fragments detected at $\theta = 2\theta_i$ arise from exploding pairs almost parallel to the surface whose initial angles between the internuclear vectors and the beam direction in the xz plane are within 20°. Although other pairs whose angles are larger than 20° also tend to be parallel to the surface as they approach the surface, fragments arising from them are hardly detected at $\theta = 2\theta_i$. With the estimation of the multiple small-angle scattering described in Sec. VII, it is estimated that more than half of the measured fragments arise from pairs whose angles between their internuclear vectors and the beam direction, Θ in Eq. (1), are within 25° throughout their trajectories. The effect of the angle Θ on the energy losses of fragments has not been shown in this work. A computer simulation taking into account the rotation of the internuclear vector is needed for an accurate calculation of the energy losses of fragments.

B. Incidence-angle dependence of the energy-loss ratio

The well-known vicinage effect on the stopping power, which has been measured and calculated for foil transmission of the fragments, decreases with increasing internuclear distance, while it is less than the half wavelength of the oscillatory wake $\pi V/\omega_p$ [4,5]. The internuclear distance at the glancing-angle scattering is mostly determined by the time the projectile interacts with the surface. The internuclear distance at the scattering decreases with an increasing angle of incidence. Therefore, one may expect from the internuclear-distance dependence of the vicinage effect that the energy-loss ratios shown in Fig. 3 increase with an increasing angle of incidence. The observed ratios shown in Fig. 3 are, however, almost constant for the angle of incidence.

The independence of the ratio from the angle of incidence is related to the dependence of the vicinage effect on the distance from the surface. Since the ion trajectories are long at the distance closest to the surface, most of the energy-loss collisions are considered to take place there. Since the energy-loss ratio does not increase as the angles of incidence increase, the vicinage effect on the stopping power may decrease as the distance from the surface decreases. The qualitative picture is expressed in Fig. 9, where the ratio of the stopping power at a small distance from the surface (typically smaller than 1 Å) shows a complicated oscillatory structure around unity. Because the typical internuclear distance at the scattering closest to the surface is several angstroms, the energy-loss ratio does not increase due to the oscillation of the ratio of stopping power, though the angle of incidence increases.

IX. CONCLUSION

Energy losses of the leading and trailing H^+ fragments arising from glancing-angle incidence of (0.15–0.6)-MeV/amu H_2^+ ions at a clean (001) surface of SnTe are measured at the angle for specular reflection. The sum of the energy losses is about 1.05–1.15 times larger than twice the energy loss of atomic H^+ ions of the same velocity. By applying the model proposed by Basbas and Ritchie and using the surface-wake potential, the energy losses of an individual proton and of a pair of protons aligned with the incident beam direction were calculated. From the calculated stopping power, the dependence of the vicinage effect on the distance from the surface is discussed. Although the dependence could not be derived by the experimental data, the agreement of the calculated energy losses with those measured supports indirectly the calculated dependence of the vicinage effects.

ACKNOWLEDGMENTS

The author is grateful to the members of the Department of Nuclear Engineering of Kyoto University for the use of the 4-MV Van de Graaff accelerator. The author is indebted to Professor M. Mannami and Professor K. Kimura for the use of their experimental apparatus for the measurements. The author would like to express sincere gratitude to Professor R. H. Ritchie and Professor J. Burgdörfer for their helpful suggestions and encouragement.

[1] D. S. Gemmell, Chem. Rev. **80**, 301 (1980); D. S. Gemmell and Z. Vager, in *Treatise on Heavy-Ion Science*, edited by D. A. Bromley (Plenum, New York, 1985), Vol. 6, p. 243.
[2] Z. Vager and D. S. Gemmell, Phys. Rev. Lett. **37**, 1352 (1976).
[3] P. J. Cooney, D. S. Gemmell, W. J. Pietsch, A. Ratkowski, Z. Vager, and B. J. Zabransky, Phys. Rev. A **24**, 746 (1981).
[4] W. Brandt, A. Ratkowski, and R. H. Ritchie, Phys. Rev. Lett. **33**, 1325 (1974).
[5] W. Brandt and R. H. Ritchie, Nucl. Instrum. Methods **132**, 43 (1976).
[6] J. W. Tape, W. H. Gibson, J. Remillieux, R. Laubert, and H. E. Wegner, Nucl. Instrum. Methods **132**, 75 (1976).
[7] A. R. Nyaiesh, W. Steckelmacher, and M. W. Lucas, J. Phys. C **11**, 2917 (1978).
[8] R. Laubert, IEEE Trans. Nucl. Sci. **26**, 1020 (1979).
[9] M. F. Steuer, D. S. Gemmell, E. P. Kanter, and B. J. Zabran-

sky, IEEE Trans. Nucl. Sci. **NS-30**, 1069 (1983).
[10] E. Ray, R. Kirsch, H. H. Mikkelsen, J.-C. Poizat, and J. Remillieux, Nucl. Instrum. Methods Phys. Res. B **69**, 133 (1992).
[11] M. Fritz, K. Kimura, Y. Susuki, and M. Mannami, Phys. Rev. A **50**, 2405 (1994).
[12] N. R. Arista and V. H. Ponce, J. Phys. C **8**, L188 (1975).
[13] N. R. Arista, Phys. Rev. B **18**, 1 (1978).
[14] J. Steinbeck and K. Dettmann, J. Phys. C **11**, 2907 (1978).
[15] J. Steinbeck, M. W. Lucas, J. Kemmiler, and K.-O. Groeneveld, Nucl. Instrum. Methods Phys. Res. B **48**, 51 (1990).
[16] J. Basbas and R. H. Ritchie, Phys. Rev. A **25**, 1943 (1982).
[17] T. Kaneko, Phys. Rev. A **51**, 535 (1995).
[18] A. Lurio, H. H. Andersen, and L. C. Feldman, Phys. Rev. A **17**, 90 (1978).
[19] Y. Susuki, H. Mukai, K. Kimura, and M. Mannami, J. Phys. Soc. Jpn. **59**, 1211 (1990).
[20] Y. Susuki, T. Ito, K. Kimura, and M. Mannami, Nucl. Instrum. Methods Phys. Res. B **90**, 310 (1994).
[21] M. Mannami, K. Kimura, K. Nakanishi, and A. Nishimura, Nucl. Instrum. Methods Phys. Res. B **13**, 587 (1986).
[22] K. Kimura, H. Ohtuka, K. Ohsima, and M. Mannami, Nucl. Instrum. Methods Phys. Res. B **90**, 227 (1994).
[23] E. P. Kanter, P. J. Cooney, D. S. Gemmell, K.-O. Groeneveld, W. J. Pietsch, A. J. Ratkowski, Z. Vager, and B. J. Zabransky, Phys. Rev. **20**, 834 (1979).
[24] Y. Susuki, T. Ito, K. Kimura, and M. Mannami, J. Phys. Soc. Jpn. **61**, 3535 (1992).
[25] D. S. Gemmell, Rev. Mod. Phys. **46**, 129 (1974).
[26] Y. Susuki, T. Ito, K. Kimura, and M. Mannami, Phys. Rev. A **51**, 528 (1995).
[27] See, for example, J. D. Jackson, *Classical Electro-Dynamics*, 2nd ed. (Wiley, New York, 1975), Chap. 13.
[28] N. Bohr, K. Dan. Vidensk. Selsk. Mat. Fys. Medd. **18**, No. 8 (1948).
[29] F. Flores and F. Garcia-Moliner, J. Phys. C **12**, 907 (1979).
[30] N. Takimoto, Phys. Rev. **146**, 366 (1966).
[31] H. Herman and S. Skillmann, *Atomic Structure Calculations* (Prentice-Hall, Englewood Cliffs, NJ, 1963).
[32] K. Narumi, Y. Fujii, K. Kishine, H. Kurakake, K. Kimura, and M. Mannami, Surf. Sci. **293**, 152 (1993).
[33] H. Finkenrath and G. H. Schafer, Phys. Status Solidi **34**, K95 (1969).
[34] D. M. Korn and R. Braunstein, Phys. Rev. B **5**, 4837 (1972).
[35] We have measured the mean initial internuclear distance from a foil-induced dissociation experiment using three carbon foils of thickness 2.1, 2.3, and 2.8 μg/cm^2 and 1-MeV H_2^+ ions. The internuclear separation R_0 can be obtained based on a calculation assuming a Coulomb explosion in free space as $R_0 = 8E_i e^2/(E_{\rm sep})^2$ (cgs esu), where E_i is the energy per a proton of incident H_2^+ and $E_{\rm sep}$ is the measured energy separation between the leading and trailing H^+ fragments, which is 6.80 keV.
[36] D. Mathur, J. B. Hasted, and S. U. Khan, J. Phys. B **12**, 2043 (1979).
[37] W. L. Fite and R. T. Brackmann, Phys. Rev. **112**, 1141 (1958).
[38] Y. Fujii, K. Sueoka, K. Kimura, and M. Mannami, J. Phys. Soc. Jpn. **58**, 2758 (1989).
[39] Y. Susuki, M. Fritz, K. Kimura, M. Mannami, N. Sakamoto, H. Ogawa, I. Katayama, T. Noro, and H. Ikegami, Phys. Rev. A **50**, 3533 (1994).
[40] I. Plesser, Nucl. Instrum. Methods **194**, 269 (1982).
[41] P. Sigmund, Nucl. Instrum. Methods Phys. Res. B **67**, 11 (1992).
[42] V. I. Shulga and P. Sigmund, Nucl. Instrum. Methods Phys. Res. B **88**, 97 (1994).
[43] K. Kimura and M. Mannami, Nucl. Instrum. Methods Phys. Res. B **27**, 442 (1987).
[44] N. R. Arista, Phys. Rev. A **49**, 1885 (1994).
[45] M. Kitagawa, Nucl. Instrum. Methods Phys. Res. B **33**, 409 (1988).